



Power Electronic Systems  
Laboratory

© 2014 IEEE

IEEE Transactions on Industrial Electronics, Vol. 61, No. 5, pp. 2236-2243, May 2014

## Optimization and Performance Evaluation of an AC-Chopper Ballast

F. Giezendanner,  
J. Biela,  
J. W. Kolar

This material is published in order to provide access to research results of the Power Electronic Systems Laboratory / D-ITET / ETH Zurich. Internal or personal use of this material is permitted. However, permission to reprint/republish this material for advertising or promotional purposes or for creating new collective works for resale or redistribution must be obtained from the copyright holder. By choosing to view this document, you agree to all provisions of the copyright laws protecting it.



Eidgenössische Technische Hochschule Zürich  
Swiss Federal Institute of Technology Zurich

# Optimization and Performance Evaluation of an AC-Chopper Ballast for HPS Lamps

Florian Giezendanner, *Member, IEEE*, Jürgen Biela, *Member, IEEE*, and Johann W. Kolar, *Fellow, IEEE*

**Abstract**—Electronic ballasts for high-pressure sodium lamps based on an ac-chopper topology are proposed as a cheaper and less complex alternative to the industry-standard low-frequency square-wave ballasts. In this paper, the design process of the ac-chopper ballast is reviewed, and the design tradeoffs caused by the single-stage topology are discussed. The analytical and simulation results are verified with measurements of a 250-W prototype system, including a detailed list of the losses for the different circuit components and electromagnetic compatibility measurements. Due to the disadvantages of the single-stage topology, a comparison to a two-stage ballast using the inverter stage of the ac-chopper ballast with a separate power factor correction stage is provided.

**Index Terms**—High-pressure sodium (HPS) lamp, lamp ballast, single stage.

## I. INTRODUCTION

HIGH-PRESSURE sodium (HPS) lamps see widespread use for public lighting applications due to their high luminous efficacy and long lifetime. Like other types of high-intensity discharge (HID) lamps, HPS lamps have a negative resistance characteristic and require a ballast to limit the lamp current during operation. Additionally, an igniter is required to start the lamp arc with voltage pulses in the range of several kilovolts. For reasons of cost and reliability, HPS lamps are usually operated with electromagnetic ballasts. However, electromagnetic ballasts have several disadvantages, including a poor power factor, relatively low efficiency, light flicker, and poor power regulation. Electronic ballasts avoid most or all of the problems depending on the employed circuit topology. The main challenge for using electronic ballasts with HID lamps is that the high-frequency (HF) operation can excite acoustic resonances in the lamp which can potentially lead to the destruction of the lamp. Even a small amount of current ripple can trigger a resonance if the switching frequency coincides with the frequency of a resonance mode [1].

Several approaches have been published to avoid acoustic resonances in HID lamps: The most common is supplying the

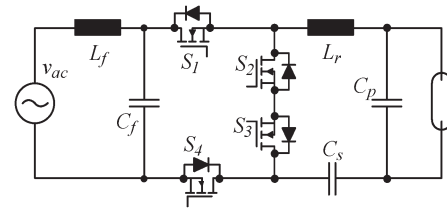


Fig. 1. AC-chopper ballast topology (complete EMC filter shown in Fig. 14).

lamp with a low-frequency square-wave (LFSQ) current [2], [3]. The main disadvantage is the circuit complexity of the two- or three-stage ballasts; however, several LFSQ ballasts with a reduced number of components have been proposed [4]–[7]. Alternatively, Tomm *et al.* [8] presented a ballast which supplies the lamp with a low-frequency sine-wave current. Further concepts include modulation schemes to avoid the excitation of the resonances [9] and operating the lamp above the resonance range. The last option is particularly interesting for HPS lamps due to the relatively low switching frequency around 120 kHz [10] compared to several megahertz for other lamp types [11].

An electronic ballast for HPS lamps based on an ac chopper (cf. Fig. 1) was presented in [12] and [13]. The converter topology has a reduced complexity compared to multistage ballasts, a high efficiency, and a potential longer lifetime because no electrolytic capacitors are required. The main disadvantage of the circuit is that, due to the missing dc-link capacitor, the sinusoidal input voltage causes a mains-frequency envelope of the HF-lamp current, resulting in light flicker and low quality of the input current due to the nonlinear characteristic of the lamp.

This paper further investigates the ac-chopper ballast to provide additional information for a potential industry application of the topology. New contributions are the investigation of a switching frequency modulation to improve the current waveforms, a detailed list of the component losses in the converter, electromagnetic compatibility (EMC) measurements, and a comparison of the losses to a two-stage ballast. Additionally, the switching frequency was increased to 120 kHz to avoid excitation of acoustic resonances. Section II explains the principle of operation for the ac-chopper ballast as presented in [12] and [13] and the effect of the nonlinear lamp characteristics on the circuit performance. In Section III, the design process for the resonant tank is shown. The input and output current waveforms can be influenced by a modulation of the switching frequency over a mains half cycle which is discussed in Section IV. Section V presents the hardware prototype including the losses for different components and EMC measurements. Finally, Section VI compares the ac-chopper ballast to a two-stage topology.

Manuscript received July 20, 2012; revised November 27, 2012 and April 24, 2013; accepted June 9, 2013. Date of publication July 24, 2013; date of current version October 18, 2013.

F. Giezendanner is with Alstom Power Sweden AB, 35242 Växjö, Sweden (e-mail: florian.giezendanner@power.alstom.com).

J. Biela is with the Laboratory for High Power Electronic Systems, Swiss Federal Institute of Technology (ETH) Zurich, 8092 Zurich, Switzerland (e-mail: jbiela@ethz.ch).

J. W. Kolar is with the Power Electronic Systems Laboratory, Swiss Federal Institute of Technology (ETH) Zurich, 8092 Zurich, Switzerland (e-mail: kolar@lem.ee.ethz.ch).

Color versions of one or more of the figures in this paper are available online at <http://ieeexplore.ieee.org>.

Digital Object Identifier 10.1109/TIE.2013.2274411

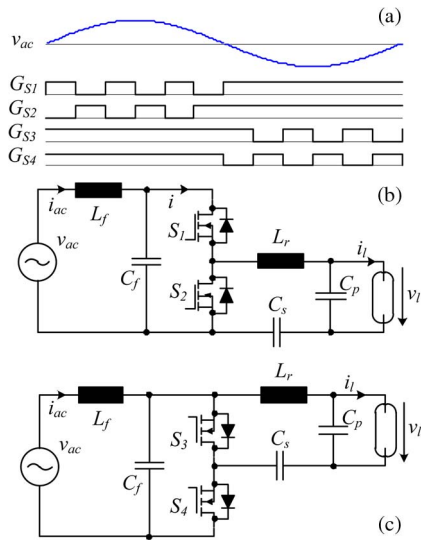


Fig. 2. (a) Gate signals of the switches for one mains cycle (low switching frequency shown to improve visibility) and equivalent circuits for (b) positive and (c) negative input voltages.

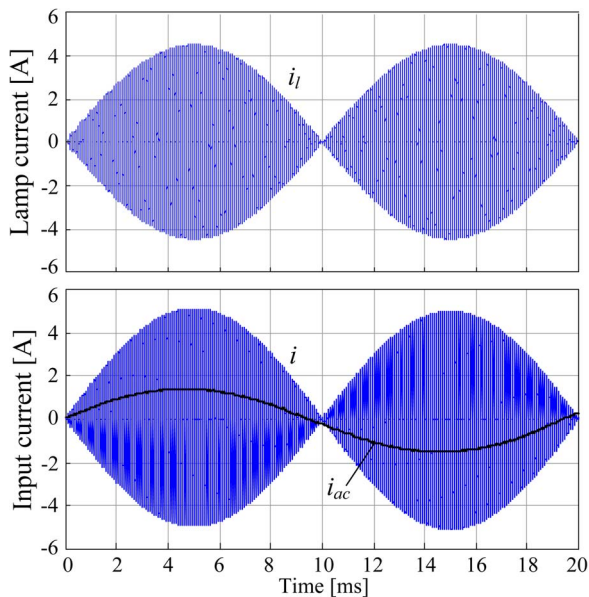


Fig. 3. Simulated output and input currents with a resistive load.

## II. PRINCIPLE OF OPERATION

The circuit consists of two half bridges  $S_1/S_2$  and  $S_3/S_4$  and an  $LCC$  series–parallel resonant tank. Fig. 2(a) shows the gate signals over a mains period. For a positive input voltage  $v_{ac}$ , MOSFETs  $S_3$  and  $S_4$  are turned on constantly while  $S_1$  and  $S_2$  are operated as a half bridge with a duty cycle of 0.5 [cf. Fig. 2(b)]. For negative half cycles,  $S_1$  and  $S_2$  are on, and  $S_3$  and  $S_4$  form the switched half bridge [cf. Fig. 2(c)].

As a result of the resonant tank, the lamp current is approximately sinusoidal with a frequency equal to the switching frequency of the half bridge. In order to avoid excitation of the acoustic resonances, the switching frequency must be above the frequency range of the resonances. Fig. 3 shows the input and output currents for a resistive load. Since the currently active

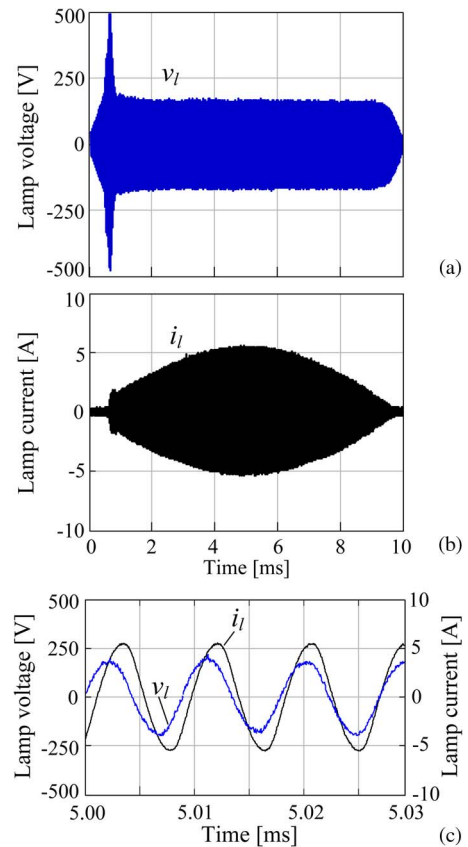


Fig. 4. Low-frequency lamp (a) voltage and (b) current waveforms with a 250-W HPS lamp and (c) HF waveforms around the peak of the mains voltage.

half bridge is supplied directly from the mains voltage, the output waveforms are modulated with the mains frequency.

The current–voltage characteristic of an HPS lamp shows a strong dependence on the operating frequency. At the mains frequency, the characteristic is highly nonlinear due to the variation of the lamp temperature over a mains half cycle. With increasing operating frequency, the lamp characteristic becomes more linear and finally shows a resistive behavior [14].

Fig. 4 shows the output voltage and current waveforms of the ballast supplying a 250-W HPS lamp. The lamp is extinguished near the zero crossing of the mains voltage until the voltage is large enough to reignite the lamp. The required voltage for reignition increases during the warm-up of the lamp. If the ballast is not able to supply the required voltage, the lamp will turn off completely.

Due to the nonlinear characteristic of the lamp, the envelope of the voltage is not sinusoidal. Fig. 5 shows the variation of the lamp resistance over a mains half period, which was calculated from the voltage and current waveforms. The decreased temperature in the lamp results in an increased resistance near the zero crossing of the mains voltage.

The impedance of the resonant inductor  $L_r$  limits the current through the lamp; therefore, no direct lamp current control is required. However, operating the lamp above the rated power has to be avoided since HPS lamps are filled with excess sodium amalgam to increase the lifetime of the lamp. Operation above the rated power evaporates additional amalgam which decreases the lamp resistance, potentially leading to a thermal runaway.

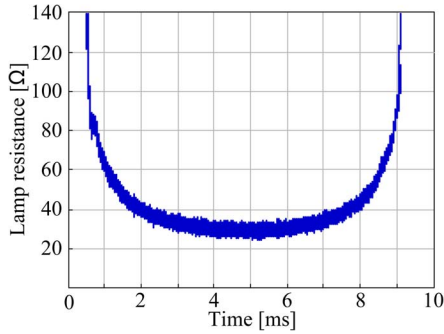


Fig. 5. Lamp resistance over a mains half cycle (calculated from the voltage and current waveforms).

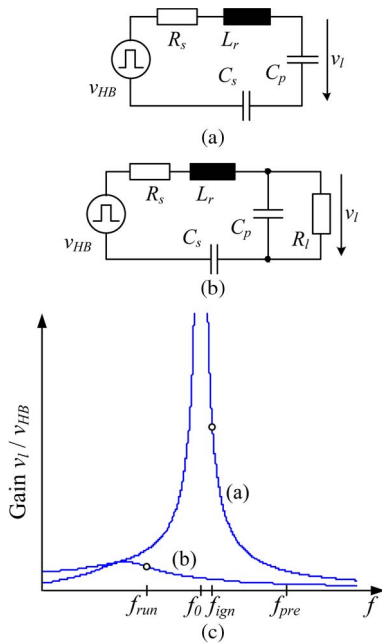


Fig. 6. Equivalent circuit of the resonant tank (a) before and (b) after ignition. (c) Calculated voltage gain curve in dependence on the equivalent lamp resistance.

### III. DESIGN OF RESONANT TANK

The performance of the ac-chopper ballast is primarily determined by the design of the *LCC* resonant tank. Fig. 6(a) and (b) shows equivalent circuits of the resonant tank before and after the ignition of the lamp, respectively. When the lamp is off, the resonant tank is only damped by the resistor  $R_s$ , consisting of the resistance of the inductor  $L_r$  and the on-resistance of the MOSFETs [cf. Fig. 6(a)]. Using a switching frequency  $f_{ign}$  close to the resonance frequency  $f_0$ , a high voltage can be created to ignite the lamp. The ignition sequence starts by operating the ballast at a switching frequency  $f_{pre}$  well above the resonance frequency. Close to the maximum of the mains voltage, an ignition pulse is then created by reducing the switching frequency to  $f_{ign}$  for 1 ms.

After the ignition of the lamp, the lamp resistance is in parallel to the capacitor  $C_p$  [cf. Fig. 6(b)] and damps the resonance. The resulting voltage gain curves are shown in Fig. 6(c). The average output current after ignition can be controlled by changing the switching frequency  $f_{run}$ .

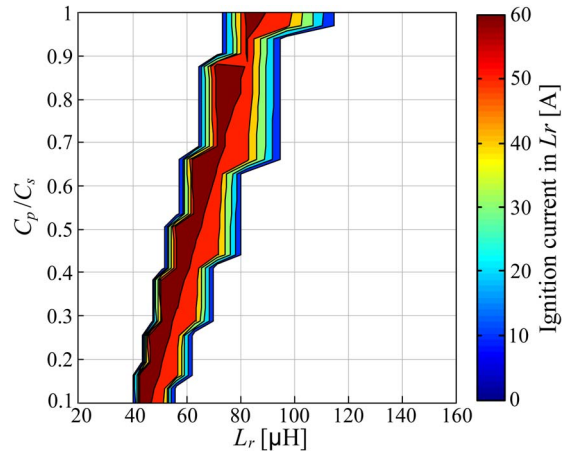


Fig. 7. Ignition current in the resonant inductor  $L_r$  for different combinations of the resonant tank components. Values exceeding the allowed current are shown in white.

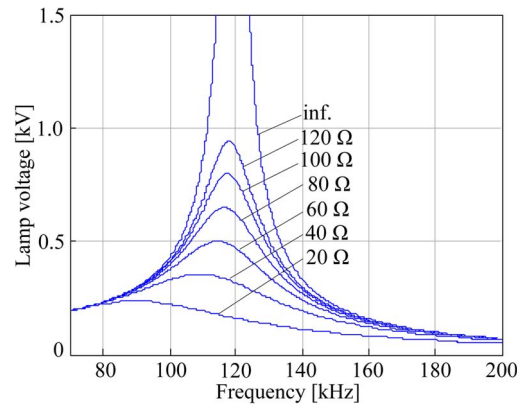


Fig. 8. Variation of the output characteristic of the resonant tank for different values of the load (cf. Fig. 5).

Due to the nearly sinusoidal waveforms, the currents and voltages in the resonant tank are calculated using the fundamental frequency analysis.

The design process starts with the definition of value ranges for the components  $L_r$ ,  $C_p$ , and  $C_s$  and the generation of a number of discrete component values within the value range. For each combination of values, the currents and voltages at ignition and in normal operation are calculated. Finally, the valid combinations are selected using the following criteria.

- 1) The maximum ignition current has to be limited in order to avoid excessive losses in the MOSFETs and saturation of the inductor  $L_r$ . As shown in Fig. 7, a maximum value of 60 A reduces the valid combinations considerably.
- 2) The minimal switching frequency has to be over 110 kHz to avoid the excitation of acoustic resonances. Additionally,  $f_{run}$  needs to be higher than the resonance frequency of the *LCC* tank to ensure zero-voltage turn-on of the MOSFETs.
- 3) The difference between the resonant frequency before ignition and that at the lowest lamp resistance is limited to 20 kHz. Larger differences lead to increased variation of the output characteristic due to the variation of the lamp resistance during a mains half cycle (cf. Figs. 5 and 8)

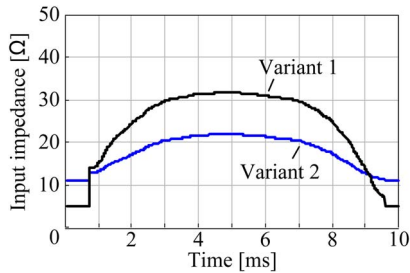


Fig. 9. Variation of the input impedance of the resonant tank over a mains half cycle. (Variant 1)  $L_r = 80 \mu\text{H}$ ,  $C_p = 35 \text{ pF}$ , and  $C_s = 55 \text{ nF}$ . (Variant 2)  $L_r = 55 \mu\text{H}$ ,  $C_p = 53 \text{ pF}$ , and  $C_s = 84 \text{ nF}$ .

which complicates the use of a switching frequency modulation.

- 4) The current in the parallel capacitor  $C_p$  has to be limited in order to avoid unnecessary losses in the switches and the resonant inductor. However, a larger capacitor decreases the variation of the input impedance over a mains half cycle (cf. Fig. 9). Therefore, there is a tradeoff between the input behavior and the efficiency of the ballast.

#### IV. SWITCHING FREQUENCY MODULATION

The behavior of the ac-chopper ballast for a given resonant tank can be influenced by a modulation of the switching frequency during a mains half period. The modulation function is implemented in the DSP as a table with 20 entries with linear interpolation in between. The modulation function allows changing the time for the lamp reignition after a zero crossing of the mains voltage by moving the switching frequency close to the resonance frequency. Furthermore, the shape of the input current can be controlled to a certain degree.

The main limitation is that there is only limited control over the lamp current close to the zero crossing of the mains voltage. Due to the high lamp resistance in this time interval, a change of the switching frequency mainly changes the current through the parallel capacitor. The second major limitation is the lack of lamp models describing the mixed low-frequency and HF operation used by the ballast. Therefore, the modulation function has to be adjusted empirically.

Fig. 10 shows measurements of the voltage and current waveforms for the prototype system with a modulation table which minimizes the length of the zero-current interval in the lamp current. The switching frequency is reduced close to the resonant frequency 0.5 ms after the zero crossing of the mains voltage to increase the voltage gain. Additionally, the switching frequency is also reduced before zero crossing to delay the extinction of the lamp as long as possible, resulting in a zero-current interval of approximately 1 ms. As shown in the input current waveform, this results in a heavy distortion of the current.

The limits of the input current harmonics for ballasts are defined in the standard IEC 61000-3-2 Class C as a percentage of the fundamental (see Table I). The diagram at the bottom of Fig. 10 shows that the limits are clearly exceeded.

Fig. 11 shows a modulation function which was modified to improve the input current shape. The reignition of the lamp is delayed which increases the zero-current interval of the lamp to about 2 ms. The input current shape is more sinusoidal than

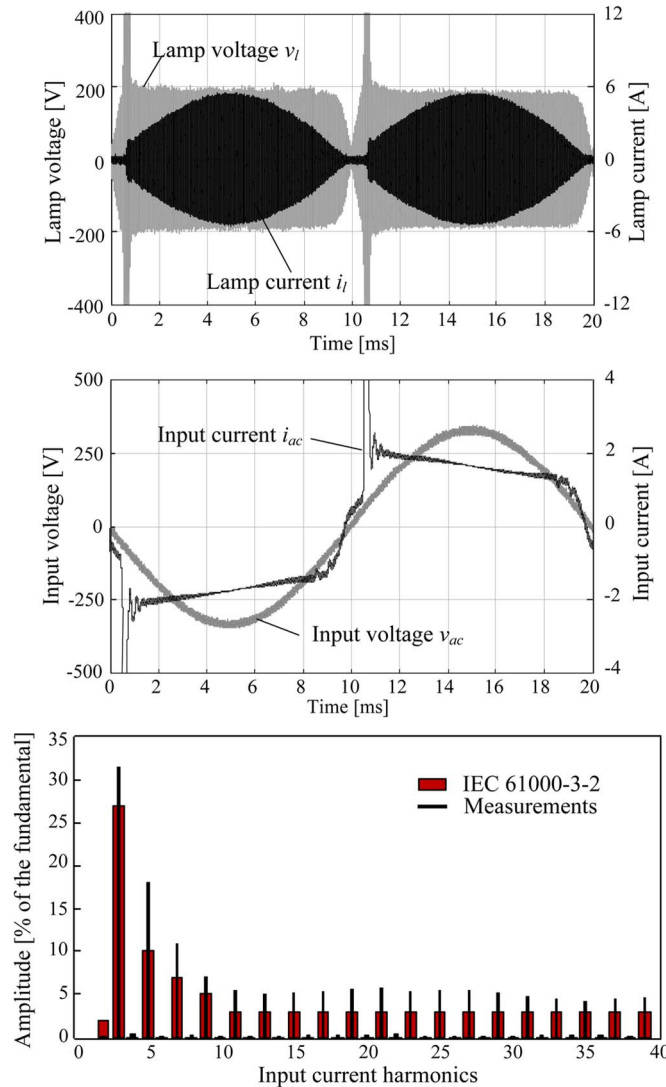


Fig. 10. Lamp and input waveforms and input harmonics for a modulation table which minimizes the zero-current interval in the lamp current to 1 ms.

TABLE I  
LIMITS OF INPUT CURRENT HARMONICS ACCORDING TO IEC 61000-3-2 CLASS C. LIMIT OF THIRD HARMONIC IS 30 TIMES POWER FACTOR

Harmonic	2	3	5	7	9	11-39
Limit [%]	2	$30 \cdot \lambda$	10	7	5	3

that in Fig. 10, but the 11th and 13th harmonics still exceed the limits.

The modulation table and the input current are shown in Fig. 12. The table was tuned experimentally with the following goals for the different parts of the mains half cycle.

- 0–1.5 ms: The switching frequency is well above the resonant frequency for the first millisecond before it is decreased to 124 kHz. This results in a delayed reignition of the lamp.
- 1.5–2.5 ms: The switching frequency is increased again to avoid the high input current in this range observed in Fig. 10.
- 2.5–8 ms: The modulation function follows approximately a sinusoidal function to shape the input current.

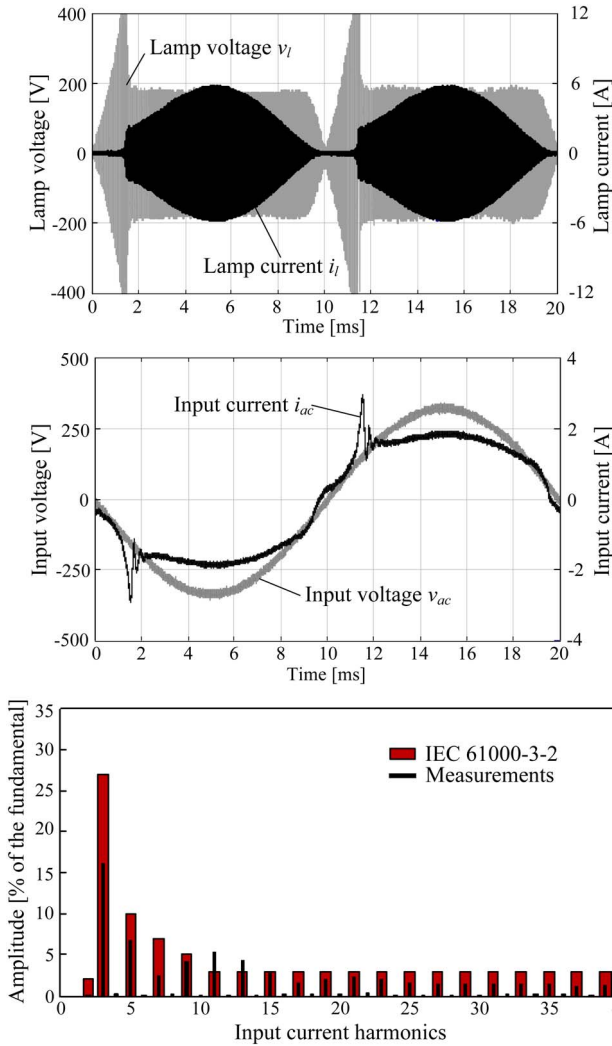


Fig. 11. Lamp and input waveforms and input harmonics for a modulation table which improves the input current shape.

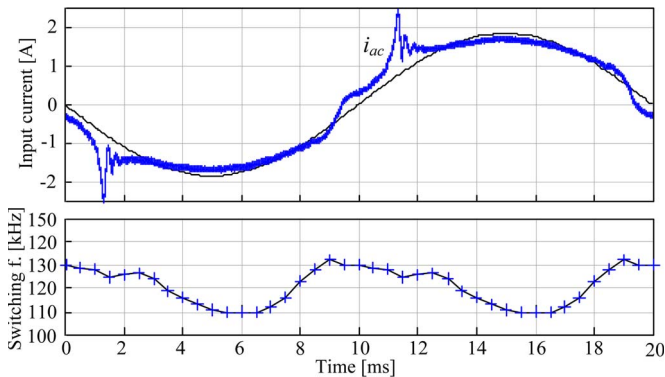


Fig. 12. Input current and modulation table. For the lower diagram, the change of the output characteristic with the lamp resistance has to be considered (cf. Figs. 5 and 8).

Due to the damping of the resonant tank, the switching frequency can be lower than the open-circuit resonant frequency.

- 4) 8–10 ms: The switching frequency is increased again for the next cycle.

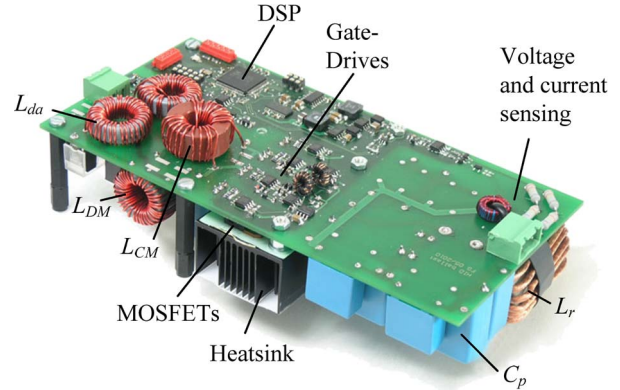


Fig. 13. Prototype of an ac-chopper ballast for a 250-W HPS lamp.

TABLE II  
COMPONENT VALUES (CF. FIG. 1)

$S_{I-A}$	-	ST STP30NM60ND
$L_r$	82 $\mu$ H	N = 27, 4xMagnetics 55326
$C_p$	35 nF	2 Epcos B3265x 2000 V (in series)
$C_s$	55 nF	Epcos B3265x 2000 V

TABLE III  
LOSSES IN BALLAST COMPONENTS

$L_r$ core	3.6 W	EMC filter	0.3 W
$L_r$ winding	0.9 W	DSP	1.2 W
$S_{I-A}$ conduction	4.4 W	Gate-drives	0.4 W
$S_{I-A}$ switching	4.5 W	Auxiliary PSU	0.4 W
$C_p$ and $C_s$	0.2 W		
Total			15.9 W
Total (measured)			17.1 W

Apart from the reignition peak, the main problem for the input current harmonics is the zero crossing which cannot be influenced by the switching frequency modulation.

The average lamp current is controlled by changing the switching frequency between 2.5 and 8 ms. The lamp current is measured using a current transformer, rectified and filtered, before it is sampled with the A/D converter of the DSP. The measured average current is compared to the reference, and a proportional–integral controller is used to provide a switching frequency value that is added to the modulation table.

Additionally, the switching of the MOSFETs is stopped if the output voltage exceeds 800 V to protect the ballast in case the lamp extinguishes or fails.

V. HARDWARE

A prototype of the ac-chopper ballast for a 250-W HPS lamp was built to verify the simulations (cf. Fig. 13). A Texas Instruments TMS320F2808 DSP used for control provides flexibility for experiments with frequency modulation. The values of the most important components (cf. Fig. 1) are listed in Table II.

Table III shows the losses of the ballast components. The switching losses were approximately calculated from eight measured points during a mains half cycle. The core losses of the resonant inductor  $L_r$  were calculated for each switching

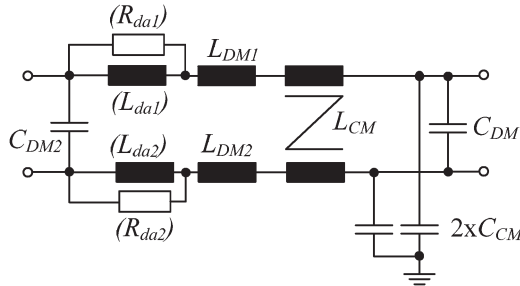


Fig. 14. Schematic of the EMC filter.

TABLE IV  
COMPONENT VALUES OF EMC FILTER

$L_{DM1,2}$	250 $\mu$ H	$C_{CM}$	20 nF
$L_{CM}$ (at 120 kHz)	2.9 mH	$(L_{da1,2})$	200 $\mu$ H
$C_{DM}$	2.2 $\mu$ F	$(R_{da1,2})$	3.5 $\Omega$
$C_{DM2}$	690 nF		

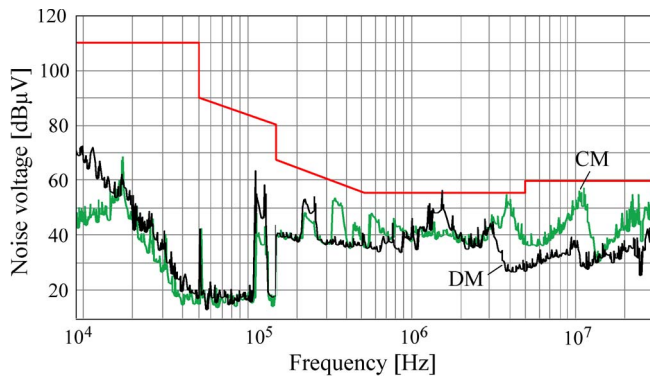


Fig. 15. Differential- and common-mode noise voltage spectra.

cycle in a circuit simulation using *GeckoCIRCUITS*, and the loss curves were provided by the core manufacturer *Magnetics*.

Additionally, the total losses were measured in a calorimeter [15]. Using the measured value, the efficiency of the ballast is 93.6%. The efficiency is reduced by the reignition of the lamp in each mains half cycle which increases the losses in the switches and the resonant inductor.

Fig. 14 shows the circuit diagram and Table IV presents the component values of the EMC filter used in the prototype, consisting of a *CLC* differential-mode filter and a *CL* common-mode filter. The relatively large value of  $C_{DM}$  is required to limit the voltage over the switches at the ignition of the lamp. Measurements showed that the input current has no significant components at the resonant frequency of  $L_{DM}$  and  $C_{DM}$ . Therefore, the damping resistors  $R_{da1}$  and  $R_{da2}$  and the bypass inductors  $L_{da1}$  and  $L_{da2}$  can be removed without affecting the performance of the ballast.

A reference ballast according to CISPR30-3 was used for the EMC measurements. Fig. 15 shows the differential- and common-mode noise components measured with a single-phase version of the noise separator presented in [16]. The relatively wide peak at the switching frequency is caused by the frequency modulation (120–130 kHz). The peak total noise voltage spectrum with automatic quasi-peak measurements shows that the requirements are fulfilled (cf. Fig. 16). For a commercial ap-

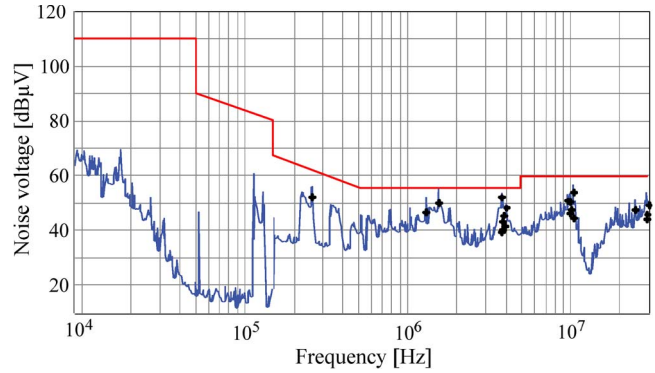


Fig. 16. Total noise voltage (peak) with (+) automatic quasi-peak measurements.

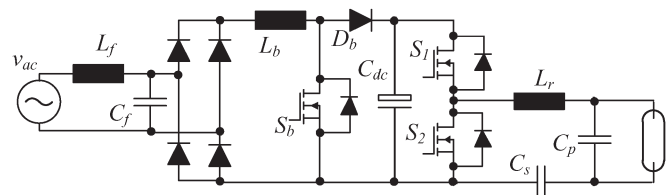


Fig. 17. Two-stage ballast topology.

TABLE V  
PFC COMPONENT VALUES (CF. FIG. 17)

$S_b$	-	Infineon IPP60R385CP
$L_b$	0.42 mH	N = 66, Epcos EFD 30 N87
$D_b$	-	Fairchild RURD660S
$C_{dc}$	100 $\mu$ F	-

TABLE VI  
LOSSES FOR TWO-STAGE BALLAST (PFC LOSSES  
ARE SIMULATED RESULTS)

$L_r$ core	3.1 W	EMC filter	0.3 W
$L_r$ winding	0.6 W	DSP	1.2 W
$S_{1,2}$ conduction	1.5 W	Gate-drives	0.3 W
$S_{1,2}$ switching	3.8 W	Auxiliary PSU	0.4 W
$C_p$ and $C_s$	0.2 W	$S_b$ conduction	0.3 W
$L_b$ core	0.5 W	$S_b$ switching	1.2 W
$L_b$ winding	0.3 W	$D_b$ conduction	0.7 W
Bridge rectifier	3.6 W		
<b>Total</b>			<b>18.0 W</b>

plication, a larger safety margin would be required to allow for tolerances of the filter components.

## VI. COMPARISON WITH TWO-STAGE BALLAST

The issues caused by the nonlinear behavior of the lamp in the ac-chopper ballast can be avoided, if the inverter stage is supplied from a dc voltage. Therefore, a two-stage ballast was investigated as a comparison, using measured data of the output stage and simulated data for the power factor correction (PFC) stage.

Fig. 17 shows the circuit diagram of the ballast combining the resonant output stage of the ac-chopper ballast with a PFC stage in boundary condition mode. Table V presents the most important PFC components used for the simulation.

The losses for the components of the two-stage ballast are shown in Table VI. Since there is no reignition of the lamp in every mains half cycle, the losses in the inverter stage are lower than those in the ac-chopper ballast. The total losses are slightly higher, but an efficiency in the range of 92%–93% should be achievable in a practical realization.

The main advantage of a two-stage ballast is that the dc-link capacitor removes the tradeoff between input and output current qualities seen in the ac-chopper ballast: With a separate PFC stage, the standards for the input current harmonics can be fulfilled, and the light of the lamp is flicker-free when the inverter is supplied from a dc-link capacitor.

Apart from the slightly higher efficiency, the main advantage of the ac-chopper ballast is that the relatively small capacitance values allow using film types for all capacitors in the power path. This can potentially increase the reliability and lifetime of the ballast, because the electrolytic dc-link capacitor is a limiting component for the lifetime of multistage ballasts [17].

## VII. CONCLUSION

The main limitation of the ac-chopper ballast is the nonlinear characteristic of the lamp due to the mains frequency envelope of the output waveforms. This results in a tradeoff between the current quality at the input and output sides and the efficiency of the converter. Modulation of the switching frequency improves the current quality, but the input current harmonic regulations could not be fulfilled with the prototype.

The main advantages of the ac-chopper topology are an efficiency of more than 93% and the lack of electrolytic capacitors, which potentially increase the reliability and lifetime of the ballast.

A comparison with a two-stage ballast based on the resonant inverter stage of the ac-chopper ballast and a boost PFC shows that a similar efficiency can be expected with fulfilled input current harmonic standards and flicker-free light output.

Due to the disadvantages of the topology, the ac-chopper ballast is limited to applications where moderate input current and light quality is acceptable.

## REFERENCES

- [1] H.-P. Stormberg and R. Schäfer, "Excitation of acoustic instabilities in discharge lamps with pulsed supply voltage," *Light. Res. Technol.*, vol. 15, no. 3, pp. 127–132, 1983.
- [2] M. Shen, Z. Qian, and F. Peng, "Design of a two-stage low-frequency square-wave electronic ballast for HID lamps," *IEEE Trans. Ind. Appl.*, vol. 39, no. 2, pp. 424–430, Mar./Apr. 2003.
- [3] F. J. Diaz, F. J. Azcondo, C. Brañas, R. Casanueva, and R. Zane, "Digitally controlled low-frequency square-wave electronic ballast with resonant ignition and power loop," *IEEE Trans. Ind. Appl.*, vol. 46, no. 6, pp. 2222–2232, Nov./Dec. 2010.
- [4] Y. Wang, D. Xu, W. Wang, X. Zhang, and B. Xu, "Electronic ballast for metal halide lamps using a quasi-resonant inverter with digital control," *IEEE Trans. Ind. Electron.*, vol. 59, no. 4, pp. 1825–1840, Apr. 2012.
- [5] R.-L. Lin and C. Lo, "Design and implementation of novel single-stage charge-pump power-factor-correction electronic ballast for metal halide lamp," *IEEE Trans. Ind. Electron.*, vol. 59, no. 4, pp. 1789–1798, Apr. 2012.
- [6] A. L. Kirsten, M. A. Dalla Costa, C. Rech, R. N. do Prado, and T. B. Marchesan, "Digital control strategy for HID lamp electronic ballasts," *IEEE Trans. Ind. Electron.*, vol. 60, no. 2, pp. 608–618, Feb. 2013.
- [7] A. L. Fuerback, C. da S. Postiglione, C. B. Nascimento, D. C. Martins, and A. J. Perin, "Near-unity power factor electronic ballast based on in-

tegration techniques to drive high-intensity discharge metal halide (HID-MH) lamps," *IEEE Trans. Ind. Electron.*, vol. 59, no. 4, pp. 1760–1769, Apr. 2012.

- [8] F. L. Tomm, A. Raniere Seidel, A. Campos, M. A. Dalla Costa, and R. N. do Prado, "HID lamp electronic ballast based on chopper converters," *IEEE Trans. Ind. Electron.*, vol. 59, no. 4, pp. 1799–1807, Apr. 2012.
- [9] J. Correa, M. Ponce, J. Arau, M. Sanchez, and J. M. Alonso, "Evaluation of frequency modulation techniques to avoid acoustic resonances in electronic ballast for HID lamps: Analysis and methodology," in *Proc. 9th IEEE Int. Power Electron. Congr.*, 2004, pp. 245–250.
- [10] F. J. Azcondo, R. Zane, and C. Brañas, "Design of resonant inverters for optimal efficiency over lamp life in electronic ballast with phase control," *IEEE Trans. Power Electron.*, vol. 22, no. 3, pp. 815–823, May 2007.
- [11] R.-L. Lin, Z.-Q. Wang, Y.-D. Lee, and F.-Y. Chen, "2.65-MHz self-oscillating complementary electronic ballast with constant-lamp-current control for a metal halide lamp," *IEEE Trans. Power Electron.*, vol. 22, no. 6, pp. 2097–2105, Nov. 2007.
- [12] G. C. R. Sincero, A. S. Franciosi, and A. J. Perin, "A 250 W high pressure sodium lamp high power factor electronic ballast using an AC chopper," in *Proc. Eur. Conf. Power Electron. Appl.*, 2005, pp. 9–10.
- [13] G. C. R. Sincero and A. J. Perin, "High pressure sodium lamp high power factor electronic ballasts using AC-AC converters," *IEEE Trans. Power Electron.*, vol. 22, no. 3, pp. 804–814, May 2007.
- [14] S. Ben-Yaakov and M. Gulko, "Design and performance of an electronic ballast for high-pressure sodium (HPS) lamps," *IEEE Trans. Ind. Electron.*, vol. 44, no. 4, pp. 486–491, Aug. 1997.
- [15] D. Christen, U. Badstübner, J. Biela, and J. W. Kolar, "Calorimetric power loss measurement for highly efficient converters," in *Proc. IEEE/IEEJ Int. Power Electron. Conf. (ECCE Asia)*, Sapporo, Japan, Jun. 21–24, 2010, pp. 1438–1445.
- [16] M. L. Heldwein, J. Biela, H. Ertl, T. Nussbaumer, and J. W. Kolar, "Novel three-phase CMDM conducted emission separator," *IEEE Trans. Power Electron.*, vol. 56, no. 9, pp. 3693–3703, Sep. 2009.
- [17] W. Yan, S. Y. R. Hui, and H. S.-H. Chung, "Energy saving of large-scale high-intensity-discharge lamp lighting networks using a central reactive power control system," *IEEE Trans. Ind. Electron.*, vol. 56, no. 8, pp. 3069–3078, Aug. 2009.



**Florian Giezendanner** (S'07–M'11) received the M.Sc. and Ph.D. degrees from the Swiss Federal Institute of Technology (ETH) Zurich, Zurich, Switzerland, in 2005 and 2012, respectively.

During his Ph.D. studies, his main research interest was the optimization of electronic lamp ballasts for fluorescent and high-pressure sodium lamps, with a focus on loss modeling and electromagnetic interference prediction. He is currently with Alstom Power Sweden AB, Växjö, Sweden, working on switching power supplies for industrial applications.



**Jürgen Biela** (S'04–M'06) received the Diploma (with honors) from Friedrich-Alexander Universität Erlangen–Nürnberg, Nuremberg, Germany, in 1999 and the Ph.D. degree from the Swiss Federal Institute of Technology (ETH) Zurich, Zurich, Switzerland, in 2006.

In 2000, he joined the Research Department, Siemens A&D, where he worked on inverters with very high switching frequencies, SiC components, and electromagnetic compatibility. In 2002, he joined the Power Electronic Systems Laboratory (PES), ETH Zurich, focusing on optimization of electromagnetically integrated resonant converters. From 2006 to 2010, he was first a Postdoctoral Fellow and then a Senior Research Associate with PES, ETH Zurich, and a Guest Researcher with the Tokyo Institute of Technology, Meguro, Japan. Since August 2010, he has been an Associate Professor of high-power electronic systems with ETH Zurich. His current research is focused on the design, modeling, and optimization of converter systems.



**Johann W. Kolar** (F'10) received the M.Sc. and Ph.D. degrees (*summa cum laude/promotio sub auspiciis praesidentis rei publicae*) from the Vienna University of Technology, Vienna, Austria.

Since 1984, he has been an Independent International Consultant in close collaboration with the Vienna University of Technology in the fields of power electronics, industrial electronics, and high-performance drives. He has proposed numerous novel converter topologies and modulation/control concepts, e.g., the Vienna rectifier, the Swiss rectifier, and the three-phase ac–ac sparse matrix converter. He has published over 550 scientific papers in international journals and conference proceedings and has filed more than 110 patents. Since February 1, 2001, he has been the Head of the Power Electronic Systems Laboratory, Swiss Federal Institute of Technology (ETH) Zurich, Zurich, Switzerland, where he was appointed as an Associate Professor in 2001 and has been a Full Professor since 2004. Since 2001, he has supervised over 60 Ph.D. students and postdoctoral fellows. He serves as an Associate Editor of the *Journal of Power Electronics* of the Korean Institute of Power Electronics and as a member of the Editorial Advisory Board of the *IEEE Transactions on Electrical and Electronic Engineering*. The focus of his current research is on ac–ac and ac–dc converter topologies with low effects on the mains, e.g., for data centers, more-electric aircraft, and distributed renewable energy systems, and on solid-state transformers for smart microgrid systems. His further main research areas are the realization of ultracompact and ultra-efficient converter modules employing latest power semiconductor technology (SiC and GaN), micro power electronics and/or power supply on chip systems, multidomain/multiscale modeling/simulation and multiobjective optimization, physical-model-based lifetime prediction, pulsed power, and ultrahigh-speed and bearingless motors. He initiated and/or is the Founder/Cofounder of four spin-off companies targeting ultrahigh-speed drives, multidomain/multilevel simulation, ultracompact/ultraefficient converter systems, and pulsed-power/electronic energy processing.

Dr. Kolar was a recipient of numerous Best Paper Awards of IEEE TRANSACTIONS and IEEE Conferences and the Golden Owl Award of the ETH Zurich for Excellence in Teaching. He is a member of the steering committees of several leading international conferences in the field and serves as an Associate Editor of the IEEE TRANSACTIONS ON POWER ELECTRONICS.